Ocean Engineering 266 (2022) 112783

Contents lists available at ScienceDirect

Ocean Engineering

journal homepage: www.elsevier.com/locate/oceaneng

On analytical solutions for transient water waves radiated by cylinders

Ruipeng Li [a,b,*], Qimeng Liu [a,b], Xiaobo Chen [c,d], Weicheng Cui [a,b]

[a] Key Laboratory of Coastal Environment and Resources of Zhejiang Province, School of Engineering, Westlake University, Hangzhou 310024, China
[b] Institute of Advanced Technology, Westlake Institute for Advanced Study, Hangzhou 310024, China
[c] Research Department, Bureau Veritas, Paris 92937, France
[d] College of Shipbuilding Engineering, Harbin Engineering University, Harbin 150001, China

ARTICLE INFO

Keywords:
Analytical solutions
Transient water waves
Potential flow theory
Cylindrical wavemaker

ABSTRACT

Analytical solutions for transient water waves radiated by a circular cylinder in deep water are studied in this paper. Within the framework of the potential flow and linear water wave theory, time-domain solutions are analytically derived based on decomposition of the velocity potential consisting of an instantaneous term and a memory term. These two terms are solved by satisfying the governing equations and initial boundary conditions. Transient concentric water waves are further studied and evaluated for a pulsating circular cylinder which expands and contracts radially. Results are compared with those from other numerical models with a good agreement in terms of wave elevation on the free surface. Analytical solutions obtained in this work can be considered as a benchmark in time-domain analysis for linear hydrodynamic problems, and are of help to the theory and application of wavemakers and transient water waves.

1. Introduction

With the dramatically fast development of deep sea exploitations and offshore engineering constructions, reliable predictions of wave-induced motions and loads on ships and marine structures are of significant importance to their designs and operations at sea. Though commercial softwares and open-source packages based on the viscous flow theory become more and more popular along with performance improvements of computers and developments of efficient algorithms (Ferziger and Peric, 2002; Moukalled et al., 2015), the potential flow theory based methodology (Newman, 1977; Faltinsen, 1990) is still widely applied to solve problems such as wave-structure interactions due to the much higher efficiency comparing with the former approach and the reasonable agreement from comparisons with experimental results. Within the framework of the potential flow theory, it is possible to obtain analytical solutions, which can be regarded as the most straightforward to study the real or simplified models comparing with either numerical simulations or physical experiments. Essential physical features and phenomena may be further revealed and explained mathematically through explicit analytical solutions.

Though frequency-domain methods are widely applied when considering rapid evaluation of prototype designs, they have limited capability for transient problems. Time-domain analysis, helpful in identifying and solving transient linear and nonlinear problems, is a direct and powerful way to give detailed descriptions of the real world, either in the theoretical analysis or in the numerical simulation. According to the ITTC (2011) report, time-domain approaches are quickly replacing frequency-domain ones for many practical applications due to advantages in the extension to the analysis of nonlinear motion and structural loads. Following the early pioneering work of Finkelstein (1957) and Cummins (1962), researchers have developed numerical methods to solve ship and marine hydrodynamic problems in the time domain. The free surface Green function is used to solve the radiation problem of a floating body with zero forward speed in Beck and Liapis (1987), with non-zero forward speed in Sen (2002). Kring (1994) applies the Rankine source to study motions of a ship travelling in waves. A hybrid method based on the fluid domain decomposition strategy is used in Liu and Papanikolaou (2011) and Tang et al. (2014), where the Rankine source is applied in the interior subdomain and the free surface Green function is used in the exterior subdomain. Besides, a high order boundary element method (HOBEM) based on bi-quadratic shape functions is employed in Chen et al. (2018b), and the Taylor Expansion Boundary Element Method (TEBEM) is utilised to solve the boundary integral equation in Chen et al. (2021). A novel multi-domain method is developed in Chen et al. (2018a) and Li et al. (2021) where the velocity potential and its radial derivative are expanded by basis functions on the mesh-free control surface. The Harmonic Polynomial Cell method is put forward in Shao and Faltinsen (2014) to solve

* Corresponding author at: Key Laboratory of Coastal Environment and Resources of Zhejiang Province, School of Engineering, Westlake University, Hangzhou 310024, China.
E-mail address: liruipeng@westlake.edu.cn (R. Li).

https://doi.org/10.1016/j.oceaneng.2022.112783
Received 14 May 2022; Received in revised form 18 September 2022; Accepted 1 October 2022

boundary value problems governed by 3D Laplace equation. However, the validation of numerical models and computer programs are done systematically by comparing with experimental data, simulation results and/or analytical solutions in frequency domain representing the steady state. The prominent advantage of time-domain approaches over frequency-domain ones to solve transient problems is weakened in some sense since real-time comparisons especially in the stage of development are missing.

Cylindrical structures are of ocean engineering interest and are common seen such as spar, tension leg platform, bridge pier, or even oscillating water columns devices for the extraction of energy from waves. Analytical solutions associated with circular cylinders are therefore fundamental and essential. Wave diffraction by a circular cylinder is first solved in Havelock (1940) for infinite water depth and in MacCamy and Fuchs (1954) for finite water depth. The scattering of water waves by an array of vertical circular cylinders is investigated in Linton and Evans (1990), the theory in which is further applied in Walker and Eatock Taylor (2005) to consider the interaction of a focused wave group with a cylinder array. An exact solution for the diffraction of short-crested waves incident on a circular cylinder is presented in Zhu (1993). Second-order wave diffraction by an array of cylinders is studied in Wang and Wu (2007) by a finite-element-based time domain method. The linearised hydrodynamic radiation problem for two concentric, free surface piercing truncated vertical cylinders is analysed in Mavrakos (2004).

Much efforts have been made to derive analytical solutions in the field of naval architecture and ocean engineering, though most of existing analytical solutions are based on frequency domain analysis and rigid assumptions for idealised geometries such as the sphere and cylinder. The added mass and damping coefficients associated with the periodic motions of a floating hemisphere are derived in Hulme (1982). Zheng and Zhang (2015) presents an analytical model based on the linearised velocity potential theory and the image theory to predict wave diffraction from a truncated cylinder in front of a vertical wall. Water wave interactions with a floating and bottom-mounted surface-piercing compound cylinder are analytically investigated based on the eigenfunction expansion method in Sarkar and Bora (2019a,b) for porous cases and in Sarkar and Bora (2020) for partial-porous cases. There are few references on analytical solutions for transient wave-structure interaction. One can be found in Dai (1998) for wave diffraction by a circular cylinder mounted on the seabed. The wavemaker problem is a typical wave-structure interaction, and a Fourier-integral method to obtain transient solutions is developed in Joo et al. (1990). Given that transient and steady-state water waves generated by motions of a cylinder or rather a cylindrical wavemaker in the water of finite depth have been derived analytically in McIver (1994) and Zou (2005), the present study is motivated to derive analytical solutions for the deep water case. They shall enrich time-domain analytical solutions of hydrodynamic problems, being of significant importance to reveal the evolution of transient waves, and to validate new developed numerical models and algorithms for time-domain hydrodynamic analyses.

The rest of this paper is organised as follows. Detailed derivations of analytical solutions for transient water waves radiated by a circular cylinder are presented in Section 2. Transient concentric waves generated by a flexible pulsating cylinder are analytically studied in terms of wave elevation and energy, numerically evaluated and illustrated in Section 3. Finally, concluding remarks are addressed in Section 4.

2. Mathematical model and its solution

We consider a semi-infinite fluid domain limited on the top by the free surface. An infinitely long circular cylinder with radius c locates vertically from the seabed to pierce the free surface and water waves are generated by any motion of this cylinder. For the sake of simplicity, a cylindrical coordinate system (r, θ, z) is introduced with $z = 0$ plane coinciding with the undisturbed free surface and oz axis orienting positively upwards, $r = 0$ being the cylinder axis as shown in Fig. 1 . The normal direction on cylinder surface $r = c$ is defined to be positive when pointing into the fluid domain, which coincides with the radial direction.

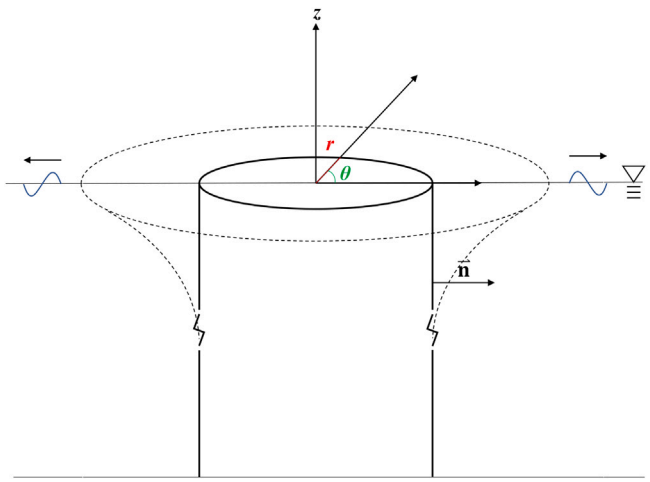

Fig. 1. Definition sketch.

In present study, the fluid is assumed inviscid, incompressible and the flow is irrotational. The surface tension at the free surface is also assumed negligible. The flow field can be described by the velocity potential Φ which is governed by the Laplace equation :

$$\nabla^2 \Phi = 0. \tag{1}$$

The exact kinematic boundary condition on the free surface gives :

$$\frac{\partial \Phi}{\partial z} = \frac{\partial \eta}{\partial t} + \frac{\partial \Phi}{\partial x}\frac{\partial \eta}{\partial x} + \frac{\partial \Phi}{\partial y}\frac{\partial \eta}{\partial y}, \quad \text{on} \quad z = \eta(x, y, t), \tag{2}$$

and the exact dynamic boundary condition on the free surface gives :

$$\eta = -\frac{1}{g}\left(\frac{\partial \Phi}{\partial t} + \frac{1}{2}\nabla\Phi \cdot \nabla\Phi\right), \quad \text{on} \quad z = \eta(x, y, t), \tag{3}$$

where $\eta(x, y, t)$ represents the vertical elevation of any point on the free surface with Cartesian coordinates $x = r\cos\theta$ and $y = r\sin\theta$, and g is the gravitational acceleration. In this study, assumptions that both small amplitude motions and small velocities of the moving cylinder, small wave heights are adopted. The wave slopes and derivatives of the velocity potential will be small quantities. Significant nonlinear effects will occur if the cylinder moves with large displacements, and this will not be discussed in this paper. It is consistent to impose the first order boundary condition on the undisturbed plane of the free surface $z = 0$. Following the linearisation of free-surface boundary conditions by neglecting the second and higher order terms (Newman, 1977; Dai, 1998), we have :

$$\frac{\partial \eta}{\partial t} = \frac{\partial \Phi}{\partial z} \quad \text{on} \quad z = 0, \tag{4}$$

and

$$\eta = -\frac{1}{g}\frac{\partial \Phi}{\partial t} \quad \text{on} \quad z = 0, \tag{5}$$

where expansions of the velocity potential and its derivatives in Taylor series about $z = 0$ are applied. From (4) and (5), the linearised boundary condition on the free surface finally gives :

$$\frac{\partial^2 \Phi}{\partial t^2} + g\frac{\partial \Phi}{\partial z} = 0, \quad \text{on} \quad z = 0. \tag{6}$$

As on the free surface, the body boundary condition is also imposed on the cylinder's mean position, $r = c$:

$$\frac{\partial \Phi}{\partial n} = V(t), \quad \text{on} \quad C, \tag{7}$$

where C denotes the average wet surface of the moving cylinder and $V(t)$ is the normal component of cylinder velocity. At infinity, we suppose there are no waves or fluid motions and we have :

$$\nabla\Phi \to 0, \quad \text{for} \quad r \to \infty \quad \text{or} \quad z \to -\infty. \tag{8}$$

To enclose the transient problem, initial conditions are given as :

$$\Phi = 0, \quad \text{at} \quad t = 0, \tag{9}$$

$$\frac{\partial \Phi}{\partial t}\Big|_{t=0} = 0, \quad \text{on} \quad z = 0. \tag{10}$$

Similar to the method proposed by Cummins (1962), applied in Dai (1998) for the transient solution of the wave diffraction around a seabed-mounted circular cylinder, the velocity potential Φ for any field point $p(r,\theta,z)$ and time t can be decomposed into two terms :

$$\Phi(p,t) = \Phi_T + \Phi_M, \tag{11}$$

with the instantaneous term Φ_T and the memory term Φ_M being :

$$\Phi_T = \iint_C \Psi(p,q)V(t)\mathrm{d}S, \tag{12a}$$

$$\Phi_M = \int_0^t \iint_C \chi(p,q,t-\tau)V(\tau)\mathrm{d}S\mathrm{d}\tau, \tag{12b}$$

where $q(c,\theta_q,z_q)$ represents a source point on C. Furthermore, Ψ in the instantaneous term Φ_T satisfies :

$$\nabla^2\Psi = 0, \tag{13a}$$

$$\Psi = 0, \quad \text{on} \quad z = 0, \tag{13b}$$

$$\frac{\partial \Psi}{\partial r} = \frac{1}{c}\delta(z-z_q)\delta(\theta-\theta_q), \quad \text{on} \quad r = c, \tag{13c}$$

$$\nabla\Psi \to 0, \quad \text{for} \quad r \to \infty \quad \text{or} \quad z \to -\infty, \tag{13d}$$

and χ in the memory term Φ_M satisfies :

$$\nabla^2\chi = 0, \tag{14a}$$

$$\frac{\partial^2\chi}{\partial t^2} + g\frac{\partial\chi}{\partial z} = 0, \quad \text{on} \quad z = 0, \tag{14b}$$

$$\frac{\partial\chi}{\partial r} = 0, \quad \text{on} \quad r = c, \tag{14c}$$

$$\nabla\chi \to 0, \quad \text{for} \quad r \to \infty \quad \text{or} \quad z \to -\infty, \tag{14d}$$

$$\chi = 0, \quad \text{at} \quad t = 0, \tag{14e}$$

$$\frac{\partial\chi}{\partial t}\Big|_{t=0} = -g\frac{\partial\Psi}{\partial z}, \quad \text{on} \quad z = 0. \tag{14f}$$

The Laplace operator ∇^2 in the cylindrical coordinate system is given as :

$$\nabla^2 \equiv \frac{1}{r}\frac{\partial}{\partial r}(r\frac{\partial}{\partial r}) + \frac{1}{r^2}\frac{\partial^2}{\partial\theta^2} + \frac{\partial^2}{\partial z^2}. \tag{15}$$

By applying the method of variable separation in (15) and boundary conditions in (13), and using the following identities associated with the Dirac delta function (Jeffrey and Dai, 2008),

$$\delta(\theta-\theta_q) = \frac{1}{2\pi}\sum_{n=0}^{\infty}\epsilon_n\cos[n(\theta-\theta_q)], \quad \epsilon_0 = 1, \quad \epsilon_n = 2(n \geq 1), \tag{16a}$$

$$\delta(z-z_q) = \frac{1}{2\pi}\int_{-\infty}^{\infty}\mathrm{e}^{\mathrm{i}k(z-z_q)}\mathrm{d}k = \frac{2}{\pi}\int_0^{\infty}\sin(kz)\sin(kz_q)\mathrm{d}k, \tag{16b}$$

the term Ψ can be solved and expressed as :

$$\Psi(p,q) = \frac{1}{\pi^2 c}\sum_{n=0}^{\infty}\Theta_n(\theta,\theta_q)\int_0^{\infty}\frac{K_n(kr)}{K_n'(kc)}\frac{\sin(kz)\sin(kz_q)}{k}\mathrm{d}k, \tag{17}$$

with the definition $\Theta_n(\theta,\theta_q) = \epsilon_n\cos[n(\theta-\theta_q)]$ for brevity. Here $K_n(kc)$ is the nth order modified Bessel function of the second kind, and $K_n'(kc)$ stands for the first order derivative of $K_n(kc)$ with respect to the argument (kc). It is known that terms χ and Ψ in (12) are linked by the initial boundary condition on the free surface (14f), which may be rewritten as follows after substituting (17),

$$\frac{\partial\chi}{\partial t}\Big|_{t=0} = \frac{-g}{\pi^2 c}\sum_{n=0}^{\infty}\Theta_n(\theta,\theta_q)\int_0^{\infty}\frac{K_n(kr)}{K_n'(kc)}\sin(kz_q)\mathrm{d}k. \tag{18}$$

Define an integral similar as the one in (18) by :

$$I = \int_0^{\infty}\frac{K_n(kr)}{K_n'(kc)}\mathrm{e}^{-\mathrm{i}kz}\mathrm{d}k. \tag{19}$$

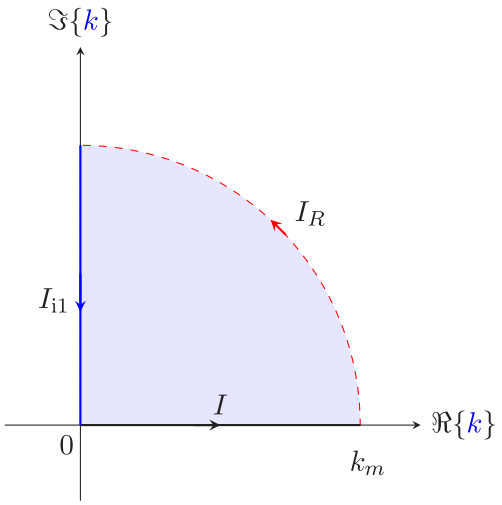

Fig. 2. Contour integral I defined by (19) in the complex k-plane, where $\Re\{\cdot\}$ and $\Im\{\cdot\}$ represent to take the real and imaginary part, respectively.

By considering the contour depicted in Fig. 2, the integrals along the complete contour are defined by that along the real k-axis I itself, that I_R along the one-quarter-circle path of radius k_m and that $I_{\mathrm{i}1}$ along the vertical path with $\Re\{k\} = 0$. According to the theorem of Cauchy about the complex contour integral (Jeffreys and Jeffreys, 1956), the sum of the above three integral is zero, namely,

$$I + I_R + I_{\mathrm{i}1} = 0. \tag{20}$$

Moreover, we may have $I = -I_{\mathrm{i}1}$ since $I_R = 0$ due to the Jordan's Lemma.

For a further evaluation of $I_{\mathrm{i}1}$ on the imaginary axis, we introduce $k = \mathrm{i}p$ and $I_{\mathrm{i}1}$ yields :

$$I_{\mathrm{i}1} = \int_{\infty}^{0}\frac{K_n(\mathrm{i}pr)}{K_n'(\mathrm{i}pc)}\mathrm{e}^{zp}\mathrm{i}\mathrm{d}p. \tag{21}$$

By using the relations between $K_n(Z)$ and the nth order Hankel functions of the second kind $H_n^{(2)}(Z)$ (Abramowitz and Stegun, 1964),

$$K_n(Z) = -\frac{\pi\mathrm{i}}{2}\mathrm{e}^{-n\pi\mathrm{i}/2}H_n^{(2)}(-\mathrm{i}Z), \quad -\frac{\pi}{2} < \arg(Z) \leq \pi. \tag{22}$$

It can be concluded that on the positive imaginary axis :

$$\frac{K_n(\mathrm{i}pr)}{K_n'(\mathrm{i}pc)} = \mathrm{i}\frac{H_n^{(2)}(pr)}{H_n^{(2)\prime}(pc)}. \tag{23}$$

By substituting (23) into (21), a new form of integral I is given as :

$$I = -\int_0^{\infty}\frac{H_n^{(2)}(kr)}{H_n^{(2)\prime}(kc)}\mathrm{e}^{kz}\mathrm{d}k. \tag{24}$$

The term associated with $H_n^{(2)}(\cdot)$ and its first order derivative $H_n^{(2)\prime}(\cdot)$ can be arranged as :

$$\frac{H_n^{(2)}(kr)}{H_n^{(2)\prime}(kc)} = F_n^{re}(k,r,c) - \mathrm{i}F_n^{im}(k,r,c), \tag{25}$$

in which,

$$F_n^{re}(k,r,c) = \Re\{\frac{H_n^{(2)}(kr)}{H_n^{(2)'}(kc)}\} = \frac{J_n(kr)J_n'(kc) + Y_n(kr)Y_n'(kc)}{[J_n'(kc)]^2 + [Y_n'(kc)]^2}, \tag{26a}$$

$$F_n^{im}(k,r,c) = -\Im\{\frac{H_n^{(2)}(kr)}{H_n^{(2)'}(kc)}\} = \frac{J_n'(kc)Y_n(kr) - J_n(kr)Y_n'(kc)}{[J_n'(kc)]^2 + [Y_n'(kc)]^2}, \tag{26b}$$

where $J_n(kc)$, $Y_n(kc)$, $J_n'(kc)$ and $Y_n'(kc)$ stands for nth order Bessel function of the first kind and second kind, and corresponding first order derivatives with respect to the argument (kc). By comparing the integral in (18) and I in (19), we have :

$$\int_0^\infty \frac{K_n(kr)}{K_n'(kc)}\sin(kz)\mathrm{d}k = -\Im\{I\} = -\int_0^\infty F_n^{im}(k,r,c)\mathrm{e}^{kz}\mathrm{d}k. \tag{27}$$

Substitute (27) into (18), the initial condition associated with χ is therefore given by :

$$\frac{\partial\chi}{\partial t}\Big|_{t=0} = \frac{g}{\pi^2 c}\sum_{n=0}^{\infty}\Theta_n(\theta,\theta_q)\int_0^\infty F_n^{im}(k,r,c)\mathrm{e}^{kz_q}\mathrm{d}k. \tag{28}$$

By using other boundary conditions and initial conditions in (14), the term χ may be further solved and expressed as :

$$\chi = \frac{g}{\pi^2 c}\sum_{n=0}^{\infty}\Theta_n(\theta,\theta_q)\int_0^\infty \mathrm{e}^{k(z+z_q)}F_n^{im}(k,r,c)\frac{\sin(\beta t)}{\beta}\mathrm{d}k, \tag{29}$$

with $\beta = \sqrt{gk}$.

As a consequence, by substituting analytical expressions of Ψ in (17) and χ in (29) into velocity potential components in (12), the instantaneous term $\boldsymbol{\Phi}_T$ yields :

$$\boldsymbol{\Phi}_T = \iint_C\left[\frac{1}{\pi^2 c}\sum_{n=0}^{\infty}\Theta_n(\theta,\theta_q)\int_0^\infty\frac{K_n(kr)}{K_n'(kc)}\frac{\sin(kz)\sin(kz_q)}{k}\mathrm{d}k\right]V(t)\mathrm{d}S, \tag{30a}$$

and the memory term $\boldsymbol{\Phi}_M$ yields :

$$\boldsymbol{\Phi}_M = \int_0^t\iint_C\frac{g}{\pi^2 c}\sum_{n=0}^{\infty}\Theta_n(\theta,\theta_q)\times \int_0^\infty \mathrm{e}^{k(z+z_q)}F_n^{im}(k,r,c)\frac{\sin[\beta(t-\tau)]}{\beta}\mathrm{d}kV(\tau)\mathrm{d}S\mathrm{d}\tau. \tag{30b}$$

The wave elevation on the free surface may be determined by :

$$\eta(r,\theta,t) = -\frac{1}{g}\frac{\partial(\boldsymbol{\Phi}_T + \boldsymbol{\Phi}_M)}{\partial t}\Big|_{z=0}. \tag{31}$$

From the expression of $\boldsymbol{\Phi}_T$ in (30a), it can be concluded that the instantaneous term $\boldsymbol{\Phi}_T$ makes no contribution to the wave elevation.

3. Results and discussions

Though any kind of motions with small amplitudes can be implemented on the circular cylinder, a periodic motion will be reported as an example in this paper. Different from the conventional rigid-body assumption, the circular cylinder in this study is assumed to be flexible and it can contract with $V(t) < 0$ and expand with $V(t) > 0$ as shown in Fig. 1.

3.1. Transient wave elevation

Supposing $S(z,\theta)$ is the stroke of the moving cylinder, the radial displacement is given as :

$$r(z,\theta,t) = -\frac{S(z,\theta)}{2}\cos(\omega t), \tag{32}$$

where ω is the wavemaker frequency. In present study, we assume the stroke of the moving cylinder $S(z,\theta)$ to take the following form for the sake of simplicity,

$$S(z,\theta) = 2A\mathrm{e}^{k_0 z}\cos(s\theta), \tag{33}$$

where the wavenumber $k_0 = \omega^2/g$ from the dispersion relationship in deep water, A represents the largest amplitude of the moving cylinder can reach and s is an integer to describe strokes along the direction of circumference. From the expression given by (33), it is obvious that the amplitude or stroke decays exponentially with the increase of vertical position z, when ignoring circumferential variances. By substituting (33) into (32), the radial displacement yields :

$$r(z,\theta,t) = -A\mathrm{e}^{k_0 z}\cos(\omega t)\cos(s\theta), \tag{34}$$

and the normal velocity $V(t)$ in (30) turns out to be :

$$V(t) = \frac{Agk_0}{\omega}\mathrm{e}^{k_0 z}\sin(\omega t)\cos(s\theta), \tag{35}$$

then the instantaneous term $\boldsymbol{\Phi}_T$ and the memory term $\boldsymbol{\Phi}_M$ in (30) are :

$$\boldsymbol{\Phi}_T = \frac{-2Agk_0}{\omega\pi}\sin(\omega t)\cos(s\theta)\int_0^\infty\frac{K_s(kr)}{K_s'(kc)}\frac{\sin(kz)}{k^2+k_0^2}\mathrm{d}k, \tag{36a}$$

$$\boldsymbol{\Phi}_M = \frac{2Agk_0}{\omega\pi}\cos(s\theta)\int_0^\infty \mathrm{e}^{kz}\frac{F_s^{im}(k,r,c)}{k+k_0}\frac{\beta\sin(\omega t) - \omega\sin(\beta t)}{\beta(k-k_0)}\mathrm{d}k. \tag{36b}$$

The wave elevation on the free surface non-dimensionalised by the largest amplitude A introduced in (33) may be obtained only from the memory term $\boldsymbol{\Phi}_M$ and expressed as :

$$\eta(r,\theta,t) = -\frac{2k_0}{\pi}\cos(s\theta)\int_0^\infty\frac{F_s^{im}(k,r,c)}{k+k_0}\frac{\cos(\omega t) - \cos(\beta t)}{k-k_0}\mathrm{d}k. \tag{37}$$

Though the instantaneous term $\boldsymbol{\Phi}_T$ makes no contribution to the wave elevation on the free surface as discussed after (31), it is of interest to have a further analysis on the two separated terms $\boldsymbol{\Phi}_T$ and $\boldsymbol{\Phi}_M$. Define another integral by :

$$I = \int_0^\infty\frac{K_s(kr)}{K_s'(kc)}\frac{\mathrm{e}^{-\mathrm{i}kz}}{k^2+k_0^2}\mathrm{d}k. \tag{38}$$

As shown in Fig. 3, the sum of all integrals in the complete contour :

$$I + I_R + I_{\mathrm{i}1} + I_\epsilon = 0, \tag{39}$$

according to the theorem of Cauchy about the complex contour integral. The integrals $I_{\mathrm{i}1}$ and I_ϵ can be given by :

$$I_{\mathrm{i}1} = \oint_\infty^0\frac{K_s(\mathrm{i}kr)}{K_s'(\mathrm{i}kc)}\frac{\mathrm{e}^{kz}}{(\mathrm{i}k)^2+k_0^2}\mathrm{i}\mathrm{d}k = \oint_\infty^0\mathrm{i}\frac{H_s^{(2)}(kr)}{H_s^{(2)'}(kc)}\frac{\mathrm{e}^{kz}}{-k^2+k_0^2}\mathrm{i}\mathrm{d}k, \tag{40a}$$

$$I_\epsilon = \mathrm{i}(-\frac{\pi}{2}-\frac{\pi}{2})\frac{K_s(\mathrm{i}kr)}{K_s'(\mathrm{i}kc)}\frac{\mathrm{e}^{k_0 z}}{2\mathrm{i}k_0} = -\frac{\pi}{2k_0}\mathrm{i}\frac{H_s^{(2)}(k_0 r)}{H_s^{(2)'}(k_0 c)}\mathrm{e}^{k_0 z}. \tag{40b}$$

Since $I_R = 0$ due to the Jordan's Lemma, the integral I in (39) may be rewritten by :

$$I = \frac{\pi}{2k_0}\mathrm{i}\frac{H_s^{(2)}(k_0 r)}{H_s^{(2)'}(k_0 c)}\mathrm{e}^{k_0 z} + \int_0^\infty\frac{H_s^{(2)}(kr)}{H_s^{(2)'}(kc)}\frac{\mathrm{e}^{kz}}{k^2-k_0^2}\mathrm{d}k. \tag{41}$$

Therefore, the integral in (36a) may be expressed as :

$$\int_0^\infty\frac{K_s(kr)}{K_s'(kc)}\frac{\sin(kz)}{k^2+k_0^2}\mathrm{d}k = \frac{-\pi}{2k_0}F_s^{re}(k_0,r,c)\mathrm{e}^{k_0 z} + \int_0^\infty\frac{F_s^{im}(k,r,c)\mathrm{e}^{kz}}{k^2-k_0^2}\mathrm{d}k. \tag{42}$$

Moreover, $\boldsymbol{\Phi}_T$ in (36a) yields :

$$\boldsymbol{\Phi}_T = \frac{Ag}{\omega}\sin(\omega t)\cos(s\theta)[F_s^{re}(k_0,r,c)\mathrm{e}^{k_0 z} - \frac{2k_0}{\pi}\int_0^\infty\frac{F_s^{im}(k,r,c)\mathrm{e}^{kz}}{k^2-k_0^2}\mathrm{d}k]. \tag{43}$$

By comparing (43) and (36b), it is noted that the second term in (43) and the first term in (36b) will cancel out, and the final form of total velocity potential $\boldsymbol{\Phi}$ may also be given by :

$$\boldsymbol{\Phi} = Ag\cos(s\theta)\left[\frac{\sin(\omega t)}{\omega}F_s^{re}(k_0,r,c)\mathrm{e}^{k_0 z} - \frac{2k_0}{\pi}\int_0^\infty\frac{\sin(\beta t)}{\beta}\frac{F_s^{im}(k,r,c)\mathrm{e}^{kz}}{k^2-k_0^2}\mathrm{d}k\right]. \tag{44}$$

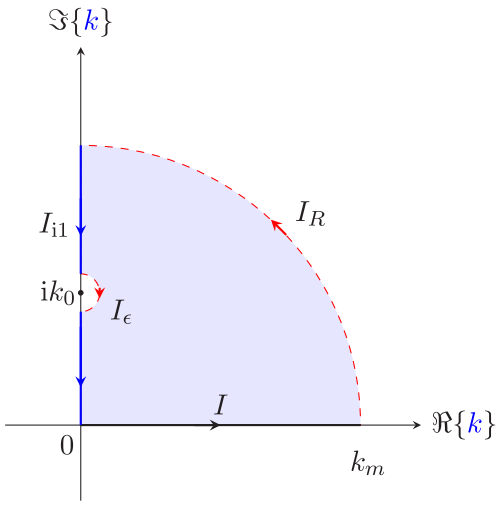

Fig. 3. Contour integral I defined by (38) in the complex k-plane.

The non-dimensional wave elevation on the free surface is then determined by (44), namely,

$$\eta = \cos(s\theta)\left[-F_s^{re}(k_0,r,c)\cos(\omega t) + \frac{2k_0}{\pi}\int_0^\infty \frac{F_s^{im}(k,r,c)}{k^2-k_0^2}\cos(\beta t)\mathrm{d}k\right], \tag{45}$$

which corresponds to the formula in (37). Referring to the implementation in Dai and He (1993), the principal value integral may be numerically dealt with as follows :

$$\int_0^\infty \frac{f(k)}{k-k_0}\mathrm{d}k = \int_0^{2k_0}\frac{f(k)-f(k_0)}{k-k_0}\mathrm{d}k + \int_{2k_0}^\infty \frac{f(k)}{k-k_0}\mathrm{d}k. \tag{46}$$

3.2. Asymptotic analysis

For analytical solutions, asymptotic forms are of interest and significance. Wave elevation on the free surface for $t \to 0$ and $t \to \infty$ will be estimated in the following content.

For $t \to 0$ which represents the initial stage, following the similar approach in Zou (2005), we expand the normal velocity $V(t)$, the velocity potential $\Phi(t)$ and the wave elevation $\eta(t)$ as follows :

$$V(t) = \sum_{n=1}^\infty \alpha_n t^n = \alpha_1 t + \alpha_2 t^2 + \alpha_3 t^3 + \cdots, \tag{47a}$$

$$\Phi(t) = \sum_{n=1}^\infty \phi_n t^n = \phi_1 t + \phi_2 t^2 + \phi_3 t^3 + \cdots, \tag{47b}$$

$$\eta(t) = \sum_{n=1}^\infty \eta_n t^n = \eta_1 t + \eta_2 t^2 + \eta_3 t^3 + \cdots. \tag{47c}$$

From the body boundary conditions of Ψ and χ, we have :

$$\frac{\partial \Phi}{\partial r} = \frac{\partial}{\partial r}\iint_C \Psi(p,q)V(t)\mathrm{d}S, \quad \text{on} \quad r = c. \tag{48}$$

By substituting (47b) and (47a) into (48), the left and right hand side terms turn out to be :

$$\mathrm{LHS} = \frac{\partial}{\partial r}\sum_{n=1}^\infty \phi_n t^n = \sum_{n=1}^\infty t^n \frac{\partial \phi_n}{\partial r}, \tag{49a}$$

$$\mathrm{RHS} = \frac{\partial}{\partial r}\iint_C \Psi(p,q)\sum_{n=1}^\infty \alpha_n t^n \mathrm{d}S = \sum_{n=1}^\infty t^n \frac{\partial}{\partial r}\iint_C \Psi(p,q)\alpha_n \mathrm{d}S \tag{49b}$$

then we have :

$$\phi_n = \iint_C \Psi(p,q)\alpha_n \mathrm{d}S, \quad \text{on} \quad r = c, \quad n = 1,2,3,\ldots. \tag{50}$$

Moreover, substituting (47b) and (47c) into the kinematic boundary condition on the free surface $\partial\eta/\partial t - \partial\Phi/\partial z = 0$, we have :

$$t^0 : \quad \eta_1 = 0, \tag{51a}$$

$$t^1 : \quad 2\eta_2 - \frac{\partial \phi_1}{\partial z} = 0, \tag{51b}$$

$$t^2 : \quad 3\eta_3 - \frac{\partial \phi_2}{\partial z} = 0, \tag{51c}$$

or equivalently,

$$\eta_1 = 0, \quad \eta_2 = \frac{1}{2}\frac{\partial \phi_1}{\partial z}, \quad \eta_3 = \frac{1}{3}\frac{\partial \phi_2}{\partial z}. \tag{52}$$

By substituting (52) and (50) into (47c), the wave elevation on the free surface for $t \to 0$ can be expressed as :

$$\begin{aligned}\eta &= \frac{1}{2}\frac{\partial \phi_1}{\partial z}\Big|_{z=0} t^2 + \frac{1}{3}\frac{\partial \phi_2}{\partial z}\Big|_{z=0} t^3 + O(t^4) \\ &= \left[\frac{\partial}{\partial z}\iint_C \Psi(p,q)(\alpha_1\frac{t^2}{2} + \alpha_2\frac{t^3}{3})\mathrm{d}S\right]_{z=0} + O(t^4).\end{aligned} \tag{53}$$

From the expansion of $V(t)$ in (47a), it is obvious that :

$$\int_0^t V(\tau)\mathrm{d}\tau = \int_0^t \sum_{n=1}^\infty \alpha_n \tau^n \mathrm{d}\tau = \sum_{n=1}^\infty \frac{\alpha_n}{n+1} t^{n+1} = \alpha_1\frac{t^2}{2} + \alpha_2\frac{t^3}{3} + \cdots. \tag{54}$$

Substitute (54) into (53), ignoring higher order quantities, then we have :

$$\eta = \left[\int_0^t \frac{\partial}{\partial z}\iint_C \Psi(p,q)V(\tau)\mathrm{d}S\mathrm{d}\tau\right]_{z=0}. \tag{55}$$

Consequently, from the expressions of Ψ in (17) and V in (35), the non-dimensional wave elevation on the free surface for $t \to 0$ is :

$$\eta(r,\theta,t) = \frac{2}{\pi}[1-\cos(\omega t)]\cos(s\theta)\int_0^\infty \frac{K_s(kr)}{K_s'(kc)}\frac{-k}{k^2+k_0^2}\mathrm{d}k. \tag{56}$$

As for $t \to \infty$, apply the dispersion relationship $\beta^2 = gk$ in (44),

$$\begin{aligned}\Phi = Ag\cos(s\theta)\Bigg[&\frac{\sin(\omega t)}{\omega}F_s^{re}(k_0,r,c)\mathrm{e}^{k_0 z} \\ &- \frac{2gk_0}{\pi}\int_0^\infty \frac{F_s^{im}(k,r,c)\mathrm{e}^{kz}}{\beta^2+\omega^2}\frac{2\sin(\beta t)}{\beta^2-\omega^2}\mathrm{d}\beta\Bigg].\end{aligned} \tag{57}$$

It can be seen that only the contribution of $\beta = \omega$ to the principal value integral needs to be estimated. Use the Taylor expansion of $\beta(k)$ at $k = k_0$,

$$\beta(k) = \beta(k_0) + \beta'(k_0)(k-k_0) + \cdots = \omega + \beta'(k_0)(k-k_0) + \cdots, \tag{58}$$

and apply the sum-difference product formula,

$$\sin(\beta t) = \sin(\omega t)\cos[t\beta'(k_0)(k-k_0)] + \cos(\omega t)\sin[t\beta'(k_0)(k-k_0)]. \tag{59}$$

From the Fourier analysis in Wehausen and Laitone (1960), the principal value integral in (57) is estimated as :

$$\lim_{t\to\infty}\int_0^\infty \frac{F_s^{im}(k,r,c)\mathrm{e}^{kz}}{\beta^2+\omega^2}\frac{2\sin(\beta t)}{\beta^2-\omega^2}\mathrm{d}\beta = \frac{\pi F_s^{im}(k_0,r,c)\mathrm{e}^{k_0 z}}{2\omega^2}\frac{\cos(\omega t)}{\omega}. \tag{60}$$

Therefore, the velocity potential for $t \to \infty$ is rewritten as :

$$\begin{aligned}\Phi &= Ag\cos(s\theta)\left[\frac{\sin(\omega t)}{\omega}F_s^{re}(k_0,r,c)\mathrm{e}^{k_0 z} - \frac{\cos(\omega t)}{\omega}F_s^{im}(k_0,r,c)\mathrm{e}^{k_0 z}\right] \\ &= \frac{Ag}{\omega}\mathrm{e}^{k_0 z}\cos(s\theta)\Im\left[\frac{H_s^{(2)}(k_0 r)}{H_s^{(2)\prime}(k_0 c)}\mathrm{e}^{\mathrm{i}\omega t}\right].\end{aligned} \tag{61}$$

The corresponding non-dimensional wave elevation on the free surface is :

$$\eta(r,\theta,t) = -\cos(s\theta)\Im\left[\mathrm{i}\frac{H_s^{(2)}(k_0 r)}{H_s^{(2)\prime}(k_0 c)}\mathrm{e}^{\mathrm{i}\omega t}\right] = -\cos(s\theta)\Re\left[\frac{H_s^{(2)}(k_0 r)}{H_s^{(2)\prime}(k_0 c)}\mathrm{e}^{\mathrm{i}\omega t}\right]. \tag{62}$$

Using the asymptotic form of Hankel function $H_s^{(2)}(k_0 r)$, we have :

$$\eta(r,\theta,t) = -\cos(s\theta)\Re\left[\frac{1}{H_s^{(2)\prime}(k_0 c)}\sqrt{\frac{2}{\pi k_0 r}}\mathrm{e}^{-\mathrm{i}(k_0 r - s\pi/2 - \pi/4)}\mathrm{e}^{\mathrm{i}\omega t}\right]. \tag{63}$$

It can be concluded that the amplitude of outgoing wave attenuates with the radial distance as $1/\sqrt{r}$. Specially, the wave elevation given in (62) represents concentric waves when $s = 0$. Or rather the circular cylinder is a pulsating wavemaker, expanding and contracting radially with no θ dependency. And the corresponding wave elevation in (63) turns out to be :

$$\eta(r,t) = \Re\left[\frac{1}{H_1^{(2)}(k_0 c)}\sqrt{\frac{2}{\pi k_0 r}}\mathrm{e}^{-\mathrm{i}(k_0 r - \omega t - \pi/4)}\right]. \tag{64}$$

Furthermore, enforce $\eta = 0$ in (64) and it is clear that :

$$\sqrt{\frac{2}{\pi k_0 r}}\frac{J_1(k_0 c)\cos\gamma + Y_1(k_0 c)\sin\gamma}{J_1^2(k_0 c) + Y_1^2(k_0 c)} = 0, \tag{65}$$

with $\gamma = k_0 r - \omega t - \pi/4$. The numerator being nil requires :

$$r_n = \frac{1}{k_0}\left[n\pi + \arctan(\Lambda) + \frac{\pi}{4} + \omega t\right], \tag{66}$$

where n is an integer and $\Lambda = -J_1(k_0 c)/Y_1(k_0 c)$. The wave length is defined as $\lambda = r_{n+2} - r_n = 2\pi/k_0$, and the wave period is $T = 2\pi/\omega$. More discussions on cylindrical wavemakers can be found in Dean and Dalrymple (1991), where three types are summarised.

3.3. Energy analysis

It is of interest to further study concentric waves from the view of energy since no literature on this has been reported to the authors' knowledge. The total energy consists of two parts, the kinetic energy due to the moving water particles, and the potential energy from displacements of the free surface. Consider the fluid in a ring band domain Ω, with radius from r_1 to r_2 with respect to the symmetry axis of the circular cylinder.

For the kinetic energy in the ring band Ω, we have :

$$\mathrm{KE} = \frac{1}{2}\rho\int_{-\pi}^{\pi}\int_{r_1}^{r_2}\int_{-\infty}^{\eta}(v_r^2 + v_z^2)r\mathrm{d}z\mathrm{d}r\mathrm{d}\theta. \tag{67}$$

From the velocity potential in (61) with $s = 0$, we have :

$$v_r = \frac{\partial\Phi}{\partial r} = \frac{Agk_0}{\omega}\mathrm{e}^{k_0 z}\cos(s\theta)\Im\left[\frac{H_0^{(2)\prime}(k_0 r)}{H_0^{(2)\prime}(k_0 c)}\mathrm{e}^{\mathrm{i}\omega t}\right], \tag{68a}$$

$$v_z = \frac{\partial\Phi}{\partial z} = \frac{Agk_0}{\omega}\mathrm{e}^{k_0 z}\cos(s\theta)\Im\left[\frac{H_0^{(2)}(k_0 r)}{H_0^{(2)\prime}(k_0 c)}\mathrm{e}^{\mathrm{i}\omega t}\right]. \tag{68b}$$

The sum of squares of v_r and v_z yields :

$$v_r^2 + v_z^2 = (\frac{Agk_0}{\omega})^2\mathrm{e}^{2k_0 z}\left\{(\Im\left[\frac{H_1^{(2)}(k_0 r)}{H_1^{(2)}(k_0 c)}\mathrm{e}^{\mathrm{i}\omega t}\right])^2 + (\Im\left[\frac{H_0^{(2)}(k_0 r)}{-H_1^{(2)}(k_0 c)}\mathrm{e}^{\mathrm{i}\omega t}\right])^2\right\}. \tag{69}$$

The integration with respect to the vertical variable z gives :

$$(\frac{Agk_0}{\omega})^2\frac{r}{2k_0}\left\{(\Im\left[\frac{H_1^{(2)}(k_0 r)}{H_1^{(2)}(k_0 c)}\mathrm{e}^{\mathrm{i}\omega t}\right])^2 + (\Im\left[\frac{H_0^{(2)}(k_0 r)}{-H_1^{(2)}(k_0 c)}\mathrm{e}^{\mathrm{i}\omega t}\right])^2\right\} + O(A^3), \tag{70}$$

where the integral is truncated up to the mean free surface retaining terms to the second order.

Substitute (70) to (67), ignoring the high order quantities, then the kinetic energy gives :

$$\mathrm{KE} = \frac{\rho\pi}{2k_0}(\frac{Agk_0}{\omega})^2\left[\mathcal{R}(r,t)\right]_{r_1}^{r_2}, \tag{71}$$

where the integral with respect to r is defined by :

$$\mathcal{R}(r,t) = \Lambda_1^2\int\left\{(\Im\left[H_1^{(2)}(k_0 r)\mathrm{e}^{\mathrm{i}\varphi}\right])^2 + (\Im\left[-H_0^{(2)}(k_0 r)\mathrm{e}^{\mathrm{i}\varphi}\right])^2\right\}r\mathrm{d}r, \tag{72}$$

with

$$\Lambda_1 = \left|\frac{1}{H_1^{(2)}(k_0 c)}\right| = \frac{1}{\sqrt{J_1^2(k_0 c) + Y_1^2(k_0 c)}}, \quad \varphi = \omega t + \arctan\frac{Y_1(k_0 c)}{J_1(k_0 c)}. \tag{73}$$

The two imaginary parts in the integrand are :

$$\Im\left[H_1^{(2)}(k_0 r)\mathrm{e}^{\mathrm{i}\varphi}\right] = J_1(k_0 r)\sin\varphi - Y_1(k_0 r)\cos\varphi, \tag{74a}$$

$$\Im\left[-H_0^{(2)}(k_0 r)\mathrm{e}^{\mathrm{i}\varphi}\right] = -J_0(k_0 r)\sin\varphi + Y_0(k_0 r)\cos\varphi. \tag{74b}$$

Substituting (74) into (72), the integrand is grouped as :

$$r\sum_{n=0}^{1}J_n^2(k_0 r)\sin^2\varphi + Y_n^2(k_0 r)\cos^2\varphi - J_n(k_0 r)Y_n(k_0 r)\sin(2\varphi). \tag{75}$$

Apply the following indefinite integral identity containing dual Bessel functions in Watson (1966),

$$\int r\mathcal{B}_n(kr)\overline{\mathcal{B}}_n(kr)\mathrm{d}r = \frac{r^2}{4}\left[2\mathcal{B}_n(kr)\overline{\mathcal{B}}_n(kr) - \mathcal{B}_{n-1}(kr)\overline{\mathcal{B}}_{n+1}(kr) - \mathcal{B}_{n+1}(kr)\overline{\mathcal{B}}_{n-1}(kr)\right], \tag{76}$$

where $\mathcal{B}$ and $\overline{\mathcal{B}}$ stand for arbitrary Bessel functions of the first or second kinds. Ignoring the arguments $(k_0 r)$ in Bessel functions, the integral $\mathcal{R}$ with respect to r yields :

$$\begin{aligned}\mathcal{R}(r,t) = {} & \Lambda_1^2\sum_{n=0}^{1}\frac{r^2}{4}\left[2J_n^2 - 2J_{n-1}J_{n+1}\right]\sin^2\varphi \\ & + \frac{r^2}{4}\left[2Y_n^2 - 2Y_{n-1}Y_{n+1}\right]\cos^2\varphi \\ & - \frac{r^2}{4}\left[2J_nY_n - J_{n-1}Y_{n+1} - J_{n+1}Y_{n-1}\right]\sin(2\varphi).\end{aligned} \tag{77}$$

The average kinetic energy can be obtained by averaging (71) over a wave period. It is obvious that :

$$\frac{1}{T}\int_{t_0}^{t_0+T}\sin^2\varphi\mathrm{d}t = \frac{1}{T}\int_{t_0}^{t_0+T}\cos^2\varphi\mathrm{d}t = \frac{1}{2}, \quad \frac{1}{T}\int_{t_0}^{t_0+T}\sin(2\varphi)\mathrm{d}t = 0. \tag{78}$$

Therefore, the average kinetic energy is expressed as :

$$\overline{\mathrm{KE}} = \frac{\rho g\pi A^2}{2}\Lambda_1^2\left[\frac{r^2}{4}\sum_{n=0}^{1}\left(J_n^2 + Y_n^2 - J_{n-1}J_{n+1} - Y_{n-1}Y_{n+1}\right)\right]_{r_1}^{r_2}. \tag{79}$$

For the potential energy in the ring band Ω, we have :

$$\mathrm{PE} = \rho g\int_{-\pi}^{\pi}\int_{r_1}^{r_2}\int_{0}^{\eta}zr\mathrm{d}z\mathrm{d}r\mathrm{d}\theta. \tag{80}$$

Substituting (62) into (80) with $s = 0$ yields :

$$\mathrm{PE} = \frac{\rho g}{2}2\pi A^2\int_{r_1}^{r_2}(\Re\left[\frac{H_0^{(2)}(k_0 r)}{H_1^{(2)\prime}(k_0 c)}\mathrm{e}^{\mathrm{i}\omega t}\right])^2 r\mathrm{d}r. \tag{81}$$

As the same notations in the kinetic energy analysis, the integration in (81) is straightforward and the corresponding indefinite integral gives :

$$\Lambda_1^2\frac{r^2}{4}\left[(2J_0^2 + 2J_1^2)\cos^2\gamma + (2Y_0^2 + 2Y_1^2)\sin^2\gamma + (2J_0Y_0 + 2J_1Y_1)\sin(2\gamma)\right]. \tag{82}$$

Similarly, the average potential energy over a wave period can be expressed as :

$$\overline{\mathrm{PE}} = \rho g\pi A^2\Lambda_1^2\left[\frac{r^2}{4}\sum_{n=0}^{1}\left(J_n^2 + Y_n^2\right)\right]_{r_1}^{r_2}. \tag{83}$$

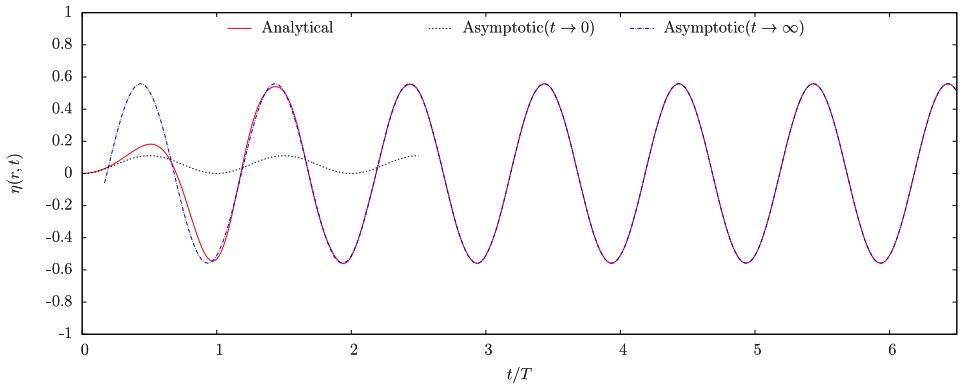

(a) $k_0c = 1.0$

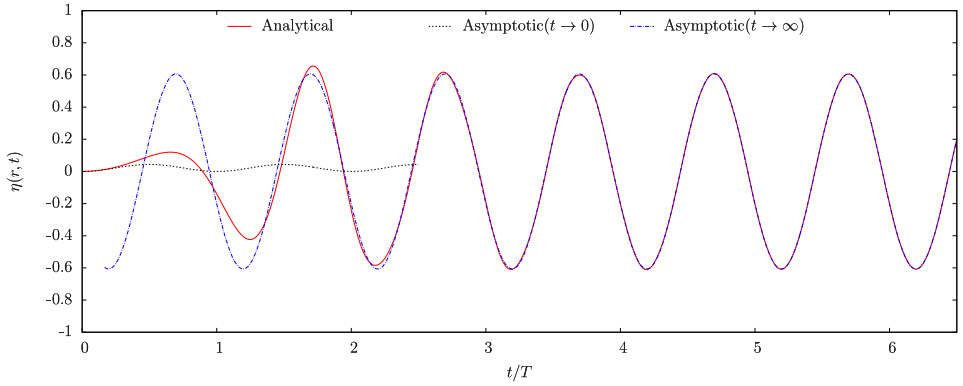

(b) $k_0c = 2.0$

Fig. 4. Comparisons of transient waves obtained from analytical and asymptotic expressions at $r = 2.5$ for $k_0c = \{1.0, 2.0\}$.

Applying only the first term of the asymptotic expansion of Bessel functions $J_n(kr)$ and $Y_n(kr)$ for large arguments (Abramowitz and Stegun, 1964),

$$\begin{pmatrix} J_n \\ Y_n \end{pmatrix}(kr) \sim \sqrt{\frac{2}{\pi kr}} \begin{pmatrix} \cos \\ \sin \end{pmatrix}(kr - \frac{n\pi}{2} - \frac{\pi}{4}), \tag{84}$$

the average kinetic and potential energy expressions are further given by :

$$\overline{\mathrm{KE}} = \frac{\rho g \pi A^2}{2} \Lambda_1^2 \left[\frac{r^2}{4} \sum_{n=0}^{1} \left(\frac{4}{\pi k_0 r} \right) \right]_{r_1}^{r_2} = \rho g A^2 \Lambda_1^2 \frac{r_2 - r_1}{k_0}, \tag{85a}$$

$$\overline{\mathrm{PE}} = \rho g \pi A^2 \Lambda_1^2 \left[\frac{r^2}{4} \sum_{n=0}^{1} \left(\frac{2}{\pi k_0 r} \right) \right]_{r_1}^{r_2} = \rho g A^2 \Lambda_1^2 \frac{r_2 - r_1}{k_0}. \tag{85b}$$

It is obvious that in a wave period, the average kinetic and potential energy are equal, and the corresponding width of the ring band $r_2 - r_1$ is identically equal to a wave length. As a consequence, the total average energy in the ring band over a wave period is :

$$\overline{\mathrm{E}} = \overline{\mathrm{KE}} + \overline{\mathrm{PE}} = \frac{4\pi\rho g A^2}{k_0^2 [J_1^2(k_0c) + Y_1^2(k_0c)]}. \tag{86}$$

3.4. Numerical results

Transient waves generated by a periodic motion of the circular cylinder are evaluated by both analytical and asymptotic expressions. As discussed in the preceding derivation, the parameter s is taken to be zero in all computations, which guarantees the waves are concentric. Or rather, the transient waves are independent with the circumferential coordinate θ.

Wave elevations varying with time instants at a radial position $r = 2.5$ are depicted in Fig. 4(a) for $k_0c = 1.0$ and Fig. 4(b) for $k_0c = 2.0$. In Fig. 4, the solid lines represent results from the analytical formulation given in (37), the dotted lines are obtained from the asymptotic expression given in (56) for a small t representing the initial stage, while the dot dashed lines are obtained from the asymptotic expression given in (62) for a large t representing the steady state. It can be seen that the developing behaviours in the very beginning of transient waves are well captured by the asymptotic expression for $t \to 0$. With time increasing, a good agreement is achieved between analytical results and those from the asymptotic expression for $t \to \infty$. The latter can be regarded as the frequency-domain solution and can provide only the steady-state wave information such as wave period. This is a very important reason to derive and study the time-domain solution, analytically in special. More characteristics on present transient concentric waves may be further analysed and revealed as the work studied in Chen and Li (2019).

Snapshots of transient waves, in terms of wave elevations on the free surface, varying with the radial coordinate r are also illustrated at four fixed time instants from $t/T = 6$ in Fig. 5(a) to $t/T = 9$ in Fig. 5(d). The dot dashed lines represent results from asymptotic expressions given in (64) for both $t \to \infty$ and $r \to \infty$. As shown in Fig. 5, a much reasonable agreement is apparently noticed between analytical and asymptotic expressions with time increasing. The wave height or amplitude is not a constant, and it varies with the order of $1/\sqrt{r}$ asymptotically as concluded in (64).

To observe the propagation of transient concentric waves more intuitively, wave elevations varying with the radial coordinate at different time instants are illustrated in Fig. 6, where lines from bottom to top represent results from $t/T = 1$ to $t/T = 20$ with the wave period $T = 2\pi/\sqrt{gk_0}$ and wave number $k_0c = 1$. The corresponding longitudinal coordinates, or rather wave elevations on the free surface, are added by a constant from 0.5 for $t/T = 2$ to 9.5 for $t/T = 20$ with an interval 0.5 to make all lines in one figure. Wave elevations at $t/T = \{5, 10, 15, 20\}$

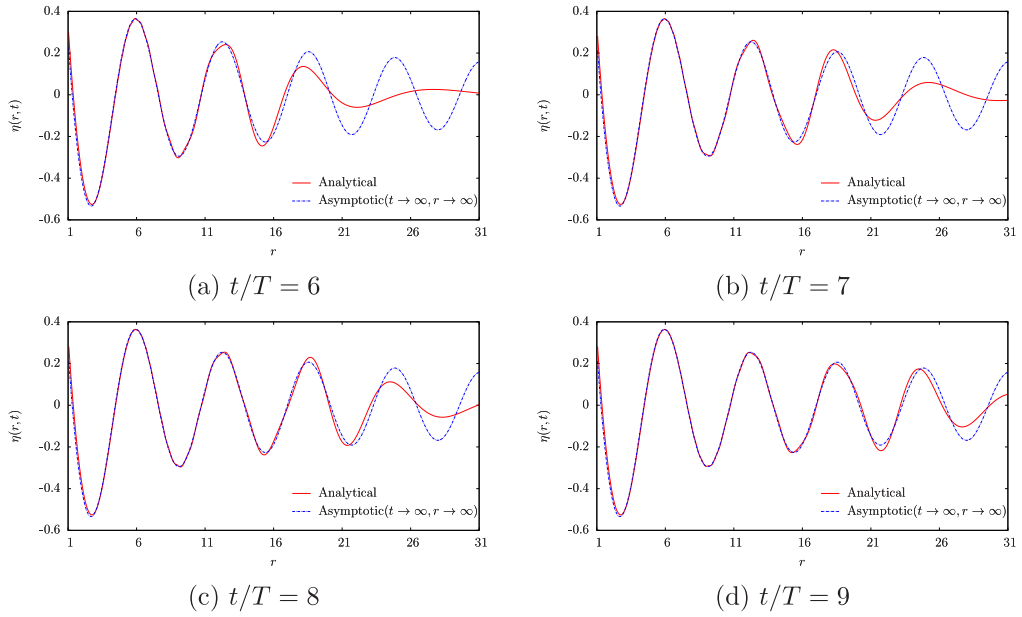

Fig. 5. Comparisons of transient waves varying with the radial distance obtained from analytical and asymptotic expressions at $t/T = \{6, 7, 8, 9\}$ for $k_0 c = 1$.

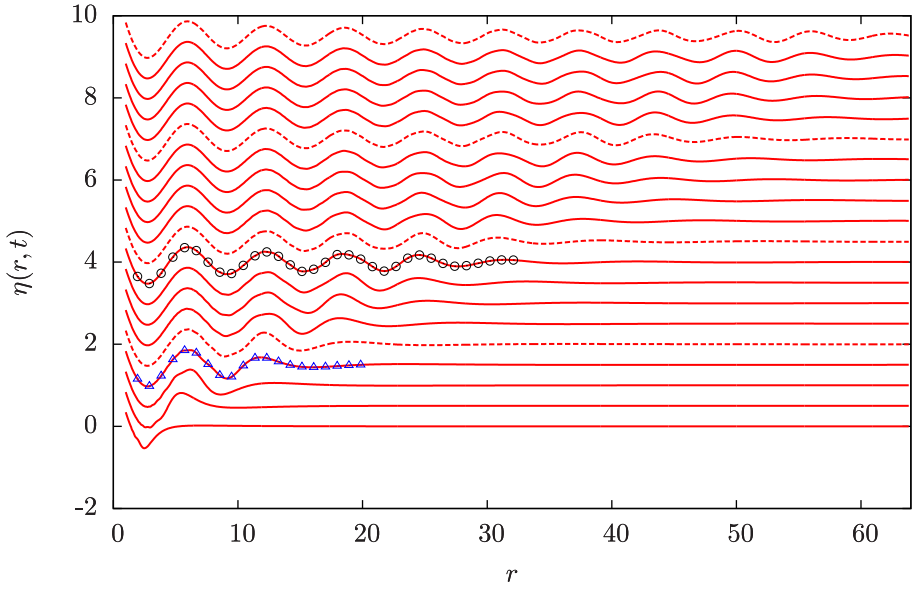

Fig. 6. Transient waves from $t/T = 1$ (bottom) to $t/T = 20$ (top) for $k_0 c = 1.0$.

are depicted by the dashed lines for a clear distinction. Moreover, numerical results obtained from the boundary integral equation, a newly developed model based on the boundary element method marked as FLBEM to study wave-structure interactions, are also shown at $t/T = 4$ and $t/T = 9$ by the triangle and circle symbols, respectively. For clarity, they are locally amplified and presented separately in Fig. 7, from which a good agreement is observed. It can be concluded that the analytical time-domain solution derived in this study may be provided as a benchmark to validate the numerical model and algorithms of high oscillatory integrals associated. More details on the numerical model FLBEM may be referred to Liang and Chen (2017), Chen et al. (2018a) and Li et al. (2021), though important expressions and the boundary integral equation have been presented in Appendix.

Wave elevations varying with time instants or the time history of wave elevations at a fixed radial position are illustrated in Fig. 8(a) for $r = 4$ and Fig. 8(b) for $r = 8$. Results from analytical solutions and those from FLBEM match well in both the initial stage and the steady state. It is worth noting that the steady amplitude for $r = 4$ does not coincide with that of $r = 8$, which is different from the case of sinusoidal plane progressive waves whose amplitudes are equal at different positions. The steady amplitude of wave elevation on the free surface can be approximately estimated as $|H_0^{(2)}(kr)/H_1^{(2)}(k_0 c)|$. It can also be observed that there exists a maximum or a minimum in the wave elevation before the transient waves reach to the steady state. Finally, to make the generated concentric waves more intuitive and visual, the contour map and corresponding perspective view at $t/T = 10$ and $t/T = 15$ are presented in Fig. 9 and Fig. 10, respectively.

It is of importance to keep in mind that present derivations, solutions and results are based on the linear free-surface boundary conditions and small amplitude water wave assumptions. In this study, the generated waves can be seen as short waves compared to the infinite water depth. For waves in deep water, the wave steepness can be used as a measure of nonlinearity of water waves. So the ratio of the wave amplitude to wave length shall be far less than one to ensure the

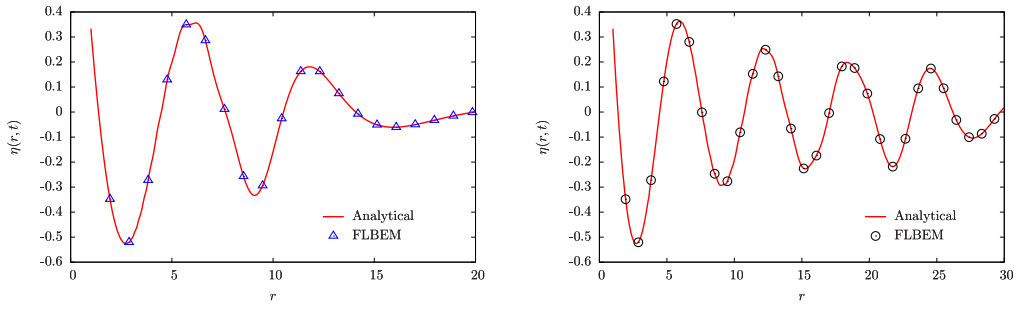

(a) $t/T = 4$ (b) $t/T = 9$

Fig. 7. Comparisons of transient waves between analytical results and those from FLBEM for $k_0 c = 1.0$.

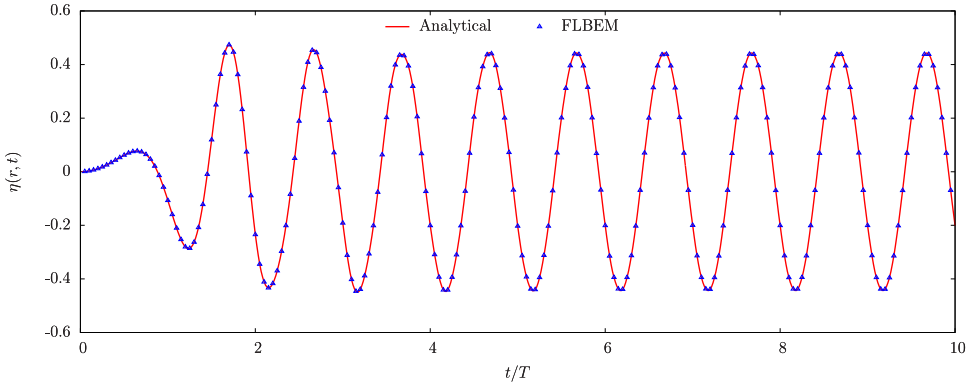

(a) $r = 4$

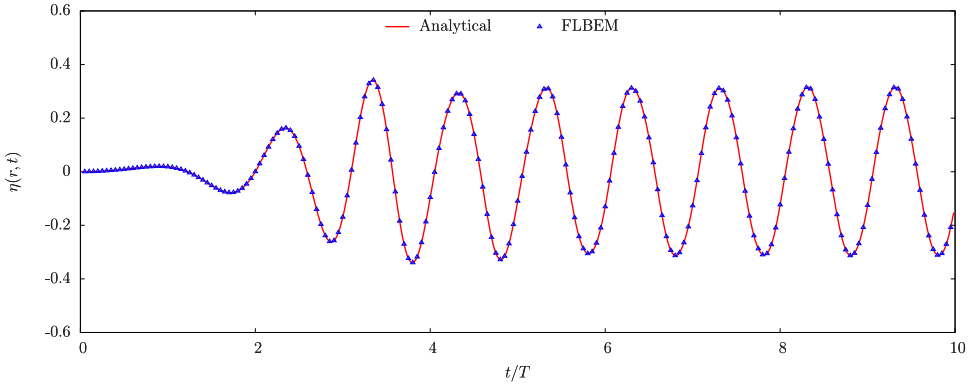

(b) $r = 8$

Fig. 8. Wave elevations varying with time instants for $k_0 c = 1.0$.

linearisation. In all the above plots and contours, the wave elevation on the free surface has been non-dimensionalised by the largest amplitude A of the moving cylinder. It is not hard to give definite values of ω and A in (32) and (33) to guarantee the wave steepness small enough and the linearisation.

4. Concluding remarks

This paper is motivated to present details on deriving analytical solutions of transient water waves generated by a moving circular cylinder. Based on the principle of pulse superposition, the total velocity potential can be decomposed into an instantaneous term and a memory term, which are further solved analytically by applying the method of variable separation and the theorem of Cauchy about the complex contour integral. The analytical time-domain solutions are evaluated and numerical results are illustrated in terms of wave elevation on the free surface for a pulsating circular cylinder, expanding and contracting radially. Results are further compared with those obtained from a recently developed numerical model based on the boundary element method in deep water and a very reasonable agreement is achieved. Analytical solutions derived in this work are of important significance for hydrodynamics in the time domain, at least from the point of view that they can be used as benchmarks for validating both numerical simulations and physical experiments. They are also helpful to generate different forms of transient water waves on the free surface and to further study propagating characteristics.

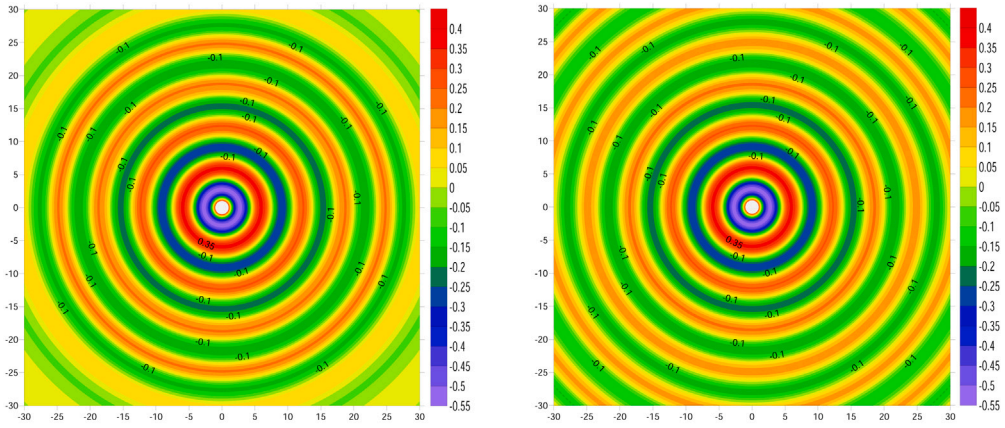

(a) $t/T = 10$ (b) $t/T = 15$

Fig. 9. Contour map of wave elevation on the free surface for $k_0 c = 1.0$.

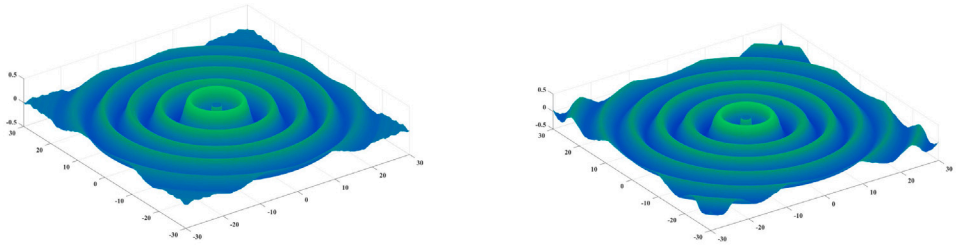

(a) $t/T = 10$ (b) $t/T = 15$

Fig. 10. Perspective view of concentric waves for $k_0 c = 1.0$.

CRediT authorship contribution statement

Ruipeng Li: Conceptualization, Software, Investigation, Writing – original draft. **Qimeng Liu:** Software, Validation, Visualization. **Xiaobo Chen:** Writing – review & editing, Methodology, Supervision. **Weicheng Cui:** Writing – review & editing, Funding acquisition.

Declaration of competing interest

The authors declare that they have no known competing financial interests or personal relationships that could have appeared to influence the work reported in this paper.

Data availability

Data will be made available on request.

Acknowledgements

This work has been partially supported by the National Natural Science Foundation of China (with project number 51779054), the Construction of a Leading Innovation Team project by the Hangzhou Municipal government, the startup funding of New-Joined PI of Westlake University (with grant number 041030150118).

Appendix. Fourier-Laguerre Boundary Element Method (FLBEM)

Applying the Green's theorem in the fluid domain limited by the free surface on the top, the cylinder surface C and a cylindrical control surface at infinity along the radial direction, the velocity potential for any field point p and time t may be given by :

$$4\pi\Phi(p,t) = \iint_C (\Phi_n G^0 - \Phi G_n^0)\mathrm{d}S + \int_0^t \left[\iint_C (\Phi_n G^f - \Phi G_n^f)\mathrm{d}S\right]\mathrm{d}\tau, \quad \text{(A.1)}$$

where the normal direction is defined positive pointing into the fluid and $\Phi_n = \partial\Phi/\partial n$. The instantaneous and memory terms of free surface time-domain Green function are :

$$G^0 = -\frac{1}{\sqrt{R^2 + (z - z_q)^2}} + \frac{1}{\sqrt{R^2 + (z + z_q)^2}}, \quad \text{(A.2a)}$$

$$G^f = -2\int_0^\infty \mathrm{e}^{k(z+z_q)} J_0(kR)\sqrt{gk}\sin[\sqrt{gk}(t-\tau)]\mathrm{d}k, \quad \text{(A.2b)}$$

where $R = \sqrt{(x-\xi)^2 + (y-\eta)^2}$ represents the horizontal distance between field point $p(r,\theta,z)$ and source point $q(c,\theta_q,z_q)$ with coordinates relations $(x,y) = r(\cos\theta, \sin\theta)$ and $(\xi,\eta) = c(\cos\theta_q, \sin\theta_q)$.

It is assumed that the velocity potential Φ and corresponding normal derivative Φ_n on the cylinder surface C are expanded by the Fourier–Laguerre series :

$$\Phi = \sum_{m=0}^{\infty}\sum_{n=-\infty}^{\infty} \phi_{mn}\mathcal{L}_m(-z)\mathrm{e}^{\mathrm{i}n\theta}, \quad \Phi_n = \sum_{m=0}^{\infty}\sum_{n=-\infty}^{\infty} \psi_{mn}\mathcal{L}_m(-z)\mathrm{e}^{\mathrm{i}n\theta}, \quad \text{(A.3)}$$

where $\mathcal{L}_m(x) = \mathrm{e}^{-x/2}L_m(x)$ with $L_m(x)$ for $x \geq 0$ standing for the mth order Laguerre polynomial defined in Abramowitz and Stegun (1964). By constructing the boundary integral equation on C in the sense of Galerkin collocation via multiplying a test function $\mathcal{L}_j(-z)\mathrm{e}^{-\mathrm{i}\ell\theta}$ on both sides of (A.1) and integrating over $(-\infty, 0)$ and $(-\pi, \pi)$ with respect to z and θ, the linear system associated with expansion coefficients ϕ_{mn} and ψ_{mn} is obtained as follows :

$$\phi_{j\ell} = \sum_{m=0}^{\infty}\sum_{n=-\infty}^{\infty} \psi_{mn}(t)\hat{G}^0_{mn,j\ell} - \phi_{mn}(t)\hat{H}^0_{mn,j\ell}$$

$$+ (\psi_{mn} * \hat{\mathcal{G}}^f_{mn,j\ell})(t) - (\phi_{mn} * \hat{\mathcal{H}}^f_{mn,j\ell})(t), \tag{A.4}$$

with notations defined by :

$$\{\hat{\mathcal{G}}^0_{mn,j\ell}, \hat{\mathcal{H}}^0_{mn,j\ell}, \hat{\mathcal{G}}^f_{mn,j\ell}, \hat{\mathcal{H}}^f_{mn,j\ell}\} = \frac{1}{4\pi} \times =$$
$$\int_{-\infty}^{0} \int_{-\pi}^{\pi} \left[\iint_C \mathcal{L}_m(-z_q) \mathrm{e}^{\mathrm{i}n\theta_q} \{G^0, G^0_n, G^f, G^f_n\} \mathrm{d}S \right] \mathcal{L}_j(-z) \mathrm{e}^{-\mathrm{i}\ell\theta} \mathrm{d}\theta \mathrm{d}z, \tag{A.5}$$

and $(\psi_{mn} * \mathcal{G}^f_{mn,j\ell})(t)$ represents the convolution of ψ_{mn} and $\mathcal{G}^f_{mn,j\ell}$, given by :

$$(\psi_{mn} * \mathcal{G}^f_{mn,j\ell})(t) = \int_0^t \psi_{mn}(\tau) \mathcal{G}^f_{mn,j\ell}(t-\tau) \mathrm{d}\tau, \tag{A.6}$$

and so does the notation of $(\phi_{mn} * \mathcal{H}^f_{mn,j\ell})(t)$. It is clear that once ψ_{mn} is given, ϕ_{mn} can be solved from the linear system (A.4), and vice versa. The expansion coefficients ψ_{mn} in (A.3) may be obtained from the corresponding inverse transformation. By using the body boundary condition $\Phi_n = V(t)$, we have :

$$\psi_{mn}(t) = \frac{1}{2\pi} \int_{-\infty}^{0} \int_{-\pi}^{\pi} V(t) \mathcal{L}_m(-z) \mathrm{e}^{-\mathrm{i}n\theta} \mathrm{d}\theta \mathrm{d}z. \tag{A.7}$$

The whole fluid domain is therefore solved and the wave elevation on the free surface may be deduced from (A.1),

$$\eta = -\frac{1}{g} \frac{\partial}{\partial t} \left[\sum_{m=0}^{\infty} \sum_{n=-\infty}^{\infty} [(\psi_{mn} * \mathcal{G}^f_{mn})(t) - (\phi_{mn} * \mathcal{H}^f_{mn})(t)] \right]_{z=0}, \tag{A.8}$$

with notations defined by :

$$(\psi_{mn} * \mathcal{G}^f_{mn})(t) = \int_0^t \psi_{mn}(\tau) \mathcal{G}^f_{mn}(t-\tau) \mathrm{d}\tau, \tag{A.9a}$$

$$\mathcal{G}^f_{mn} = \frac{1}{4\pi} \iint_C \mathcal{L}_m(-z_q) \mathrm{e}^{\mathrm{i}n\theta_q} G^f \mathrm{d}S, \tag{A.9b}$$

and so do the notations of $(\phi_{mn} * \mathcal{H}^f_{mn})(t)$ and $\mathcal{H}^f_{mn}$.

References

Abramowitz, M., Stegun, I.A., 1964. Handbook of Mathematical Functions: with Formulas, Graphs, and Mathematical Tables. National Bureau of Standards.

Beck, R.F., Liapis, S., 1987. Transient motions of floating bodies at zero forward speed. J. Ship Res. 31 (3), 164–176.

Chen, J.K., Duan, W.Y., Ma, S., Li, J.D., 2021. Time domain TEBEM method of ship motion in waves with forward speed by using impulse response function formulation. Ocean Eng. 227, 108617.

Chen, X.B., Li, R.P., 2019. Reformulation of wavenumber integrals describing transient waves. J. Eng. Math. 115, 121–140.

Chen, X.B., Liang, H., Li, R.P., Feng, X.Y., 2018a. Ship seakeeping hydrodynamics by multi-domain method. In: Proceedings of 32nd Symposium on Naval Hydrodynamics, Hamburg, Germany.

Chen, X., Zhu, R.C., Zhou, W.J., Zhao, J., 2018b. A 3D multi-domain high order boundary element method to evaluate time domain motions and added resistance of ship in waves. Ocean Eng. 159, 112–128.

Cummins, W.E., 1962. The impulsive response function and ship motions. Schiffstechnik 9, 101–109.

Dai, Y.S., 1998. Potential Flow Theory of Ship Motions in Waves in Frequency and Time Domain. National Defense Industry Press.

Dai, Y.S., He, W.Z., 1993. The transient solution of plane progressive waves. China Ocean Eng. 7 (3), 305–312.

Dean, R.G., Dalrymple, R.A., 1991. Water Wave Mechanics for Engineers and Scientists. World Scientific.

Faltinsen, O.M., 1990. Sea Loads on Ships and Offshore Structures. Cambridge University Press.

Ferziger, J.H., Peric, M., 2002. Computational Methods for Fluid Dynamics. Springer.

Finkelstein, A.B., 1957. The initial value problem for transient water waves. Comm. Pure Appl. Math. 10, 511–522.

Havelock, T.H., 1940. The pressure of water waves upon a fixed obstacle. Proc. R. Soc. Lond. A Math. Phys. Eng. Sci. 175 (963), 409–421.

Hulme, A., 1982. The wave forces acting on a floating hemisphere undergoing forced periodic oscillations. J. Fluid Mech. 121, 443–463.

ITTC, 2011. The seakeeping committee-final report and recommendations to the 26th ITTC. In: Proceedings of 26th International Towing Tank Conference, Rio de Janeiro, Brazil.

Jeffrey, A., Dai, H.-H., 2008. Handbook of Mathematical Formulas and Integrals, fourth ed. Academic Press.

Jeffreys, H., Jeffreys, B., 1956. Methods of Mathematical Physics, third ed. Cambridge University Press.

Joo, S.W., Schultz, W.W., Messiter, A.F., 1990. An analysis of the initial-value wavemaker problem. J. Fluid Mech. 214, 161–183.

Kring, D.C., 1994. Time Domain Ship Motions by a Three-Dimensional Rankine Panel Method (Ph.D. thesis). Massachusetts Institute of Technology.

Li, R.P., Chen, X.B., Duan, W.Y., 2021. Transient wave diffraction around cylinders by a novel boundary element method based on Fourier-Laguerre expansions. Ships Offshore Struct. 16 (1), 100–111.

Liang, H., Chen, X.B., 2017. A new multi-domain method based on an analytical control surface for linear and second-order mean drift wave loads on floating bodies. J. Comput. Phys. 347, 506–532.

Linton, C.M., Evans, D.V., 1990. The interaction of waves with arrays of vertical circular cylinders. J. Fluid Mech. 215, 549–569.

Liu, S.K., Papanikolaou, A.D., 2011. Time-domain hybrid method for simulating large amplitude motions of ships advancing in waves. Int. J. Nav. Archit. Ocean Eng. 3 (1), 72–79.

MacCamy, R.C., Fuchs, R.A., 1954. Wave Forces on Piles: A Diffraction Theory. Technical Memorandum No. 69, U.S. Army Coastal Engineering Research Center (Formerly Beach Erosion Board).

Mavrakos, S.A., 2004. Hydrodynamic coefficients in heave of two concentric surface-piercing truncated circular cylinders. Appl. Ocean Res. 26, 84–97.

McIver, P., 1994. Transient fluid motion due to the forced horizontal oscillations of a vertical cylinder. Appl. Ocean Res. 16, 347–351.

Moukalled, F., Mangani, L., Darwish, M., 2015. The Finite Volume Method in Computational Fluid Dynamics: An Advanced Introduction with OpenFOAM and MATLAB. Springer.

Newman, J.N., 1977. Marine Hydrodynamics. Massachusetts Institute of Technology Press.

Sarkar, A., Bora, S.N., 2019a. Hydrodynamic forces due to water wave interaction with a bottom-mounted surface-piercing compound porous cylinder. Ocean Eng. 171, 59–70.

Sarkar, A., Bora, S.N., 2019b. Water wave diffraction by a surface-piercing floating compound porous cylinder in finite depth. Geophys. Astrophys. Fluid Dyn. 113 (4), 348–376.

Sarkar, A., Bora, S.N., 2020. Hydrodynamic forces and moments due to interaction of linear water waves with truncated partial-porous cylinders in finite depth. J. Fluids Struct. 94, 102898.

Sen, D., 2002. Time-domain computation of large amplitude 3D ship motion with forward speed. Ocean Eng. 29, 973–1002.

Shao, Y.L., Faltinsen, O.M., 2014. A harmonic polynomial cell (HPC) method for 3D Laplace equation with application in marine hydrodynamics. J. Comput. Phys. 274, 312–332.

Tang, K., Zhu, R.C., Miao, G.P., Fan, J., 2014. Domain decomposition and matching for time-domain analysis of motions of ships advancing in head sea. China Ocean Eng. 28 (4), 433–444.

Walker, D., Eatock Taylor, R., 2005. Wave diffraction from linear arrays of cylinders. Ocean Eng. 32, 2053–2078.

Wang, C.Z., Wu, G.X., 2007. Time domain analysis of second-order wave diffraction by an array of vertical cylinders. J. Fluids Struct. 23, 605–631.

Watson, G.N., 1966. A Treatise on the Theory of Bessel Functions. Cambridge University Press.

Wehausen, J.V., Laitone, E.V., 1960. Surface waves. Hanbuch Phys. 9.

Zheng, S., Zhang, Y., 2015. Wave diffraction from a truncated cylinder in front of a vertical wall. Ocean Eng. 104, 329–343.

Zhu, S.P., 1993. Diffraction of short-crested waves around a circular cylinder. Ocean Eng. 20, 389–407.

Zou, Z.L., 2005. Water Wave Theories and their Applications. Scientific Press.